Supplementary Information (SI) for Journal of Materials Chemistry A.
This journal is © The Royal Society of Chemistry 2026

Supporting information

Weakening OH Adsorption on Ru Sites by Ni Alloying for Accelerating Alkaline Hydrogen Evolution of intermetallic Ru_3Ni electrocatalyst

Hui Zhang[a†], Xinyi He[b†], Jie Wang[a†], Qun Yang[b], Xueqin Zuo[b*], Huaibao Tang[b], Dongmeng Chen[b], Xiaofei Niu[d], Haifeng Xu[d*], Guang Li[a,d,*]

[a]School of Materials Science and Engineering, Anhui Key Laboratory of Information Materials and Devices, Anhui University, Hefei 230601, China

[b]School of Physics and Optoelectronic Engneering, Anhui University, Hefei 230601, China

[c]College of Science, China University of Petroleum, Qingdao 266580, China

[d]School of Electronic and Information Engineering, Hefei Institute of Technology, Hefei 238076, China

†These authors contributed equally to this work

Corresponding Authors:

*Email: Email: (Xueqin Zuo) xqzuo@ahu.edu.cn; (Haifeng Xu) xuhaifeng@hfit.edu.cn; (Guang Li) liguang1971@ahu.edu.cn

Experimental Sections

Chemicals and materials

Tetrapropyl orthosilicate (TPOS), resorcinol and ammonium hydroxide ($NH_3 \cdot H_2O$, 25%) were purchased from Aladdin; formaldehyde (37%), nickel(II) sulfate heptahydrate ($NiSO_4 \cdot 6H_2O$, ⩾98.5%). Sodium hydroxide (NaOH), potassium hydroxide (KOH, 90%) and absolute ethanol were received from Shanghai Macklin Biochemical Co, Ltd. All chemicals used without further purification. TGP-H-060 TORAY Coborn paper (CP) was purchased from Suzhou Sino Technology Co., Ltd. sulfuric acid (H_2SO_4, AR, ≤98%), acetone (C_3H_6O, AR, ≤95%) were purchased from Sinopharm Co., Ltd., Deionized water.

Synthesis of CN

First, 3.46 mL of TPOS (12 mmol) was added to the mixed solution containing 70 mL of ethanol, 10 mL of DI water and 3 mL of $NH_3 \cdot H_2O$. Then, after 15 min of stirring, 0.4 g of resorcinol and 0.56 mL of formaldehyde were casted into the solution with a further 24 h of stirring. The obtained SiO_2@SiO_2/phenolic resin (PF) precursor were collected through centrifugal washing with DI water and ethanol for three times, respectively. When the precursor was dried in vacuum oven over one night, 2 g of precursor was put into porcelain boat for high-temperature calcination under NH_3/N_2 atmosphere to convert PF into carbon material. The calcined condition set as 700 ℃ for 5 h with a ramping rate of 5 ℃/min.

Synthesis of Synthesis of Ru_3Ni/CN

50 mg NC, 15 mL water and 15 mL ethanol were added to the beaker and

ultrasonic treatment for 30 min. 4 mL $RuCl_3$ solution and 9 mL $Ni(bpy)_3SO_4$ solution (0.25 mmol and 0.75 mmol bpy in 50 ml ethanol and water mixed solution) were added. Dried at 60℃ and annealed at 400℃ in a nitrogen atmosphere.

Materials Characterizations

The structures of all Ru_3Ni/CN series samples were first examined by powder XRD on SmartLab. X-ray diffractometer with Cu Kα Radiation (λ = 1.541 Å). The morphology and structure observations of samples were conducted with TEM and HRTEM on F-200 field emission electron microscopy with an acceleration voltage of 200 kV. Atomic structures of samples were observed through HAADF-STEM on a JEOL JEM-ARF200F (200 kV) with a spherical aberration corrector. Elemental mapping was also measured. X-ray photoelectron spectroscopy (XPS) (ESCALAB-250) was used to determine the sample's chemical composition and valence state. ICP-AES measurement was used to determine the Ru loading amounts. Gas physical adsorption (BET) (ASAP 2460) was used to analyze the product's specific surface area.

In situ Raman characterization

The operando Raman spectra were collected on a LabRAM HR Evolution Raman spectrometer equipped with an excitation laser of 532 nm and an electrochemical cell, catalysts were directly dropped on glassy carbon electrode as the working electrode, calomel electrode and carbon rod were used as the reference electrode and counter electrode, respectively. It operated from 200 to 4000 cm^{-1} and 0 to -80mV vs. RHE in 1 M KOH solution to evaluate the water dissociation ability of catalysts. The specific process is as follows: 5 mg of the catalysts was added to 1000 μL of anhydrous ethanol

and 20 μL of Nafion solution (5 wt.%), and then ultrasonically dispersed for 30 minutes to obtain the catalyst ink. Dropping ink onto the pretreated electrode, we controlled the catalyst mass loading to 1.5 mg cm^{-2}. Data acquisition is carried out at room temperature.

Electrochemical measurements

All electrochemical measurements were conducted using CHI 660E potentiostat (Chenhua, China) with conventional three-electrode setup. Graphite rod, silver chloride electrode (Hg/HgO), and glassy carbon electrode (diameter: 3 mm) were used as the counter, reference, and working electrodes, respectively. Before each testing session, the glassy carbon rotating disk electrode (RDE) was polished using alumina suspension and rinsed several times with a mixture of ethanol/DI water. The silver chloride electrode was also calibrated with respect to the reversible hydrogen electrode (RHE) by recording the polarization curve of Pt-plate electrode in highly pure H2-saturated electrolytes. we used the saturated as reference electrode. Before each testing session, the glassy carbon rotating disk electrode (RDE) was polished using alumina suspension and rinsed several times with a mixture of ethanol/DI water. The linear sweep voltammetry (LSV) test was performed at a scan rate of 5 $mV \cdot s^{-1}$ after purging H_2 in the electrolyte for 20 min. All the potentials in the LSV are IR-corrected, and the resistance for IR compensation is tested at the open circuit potential. EIS test frequency range is 10^5~10^{-2} Hz unless otherwise indicated, 1.0 M potassium hydroxide solution (KOH) and 0.5 M sulfuric acid solution (H_2SO_4) were prepared as electrolytes. In the typical preparation of catalyst ink, a 5 mg catalyst sample and 50 μL of 5wt% Nafion

solution (Sigma-Aldrich) were dispersed in 700 μL water and 300 μL anhydrous ethanol mixed solvent by ultrasonic treatment for 30 min to form uniform ink. Then, the above catalyst ink was dropped on a glassy carbon electrode with a diameter of 3 mm and dried in the surrounding environment to form a catalyst film with a mass load of 0.25 $mg \cdot cm^{-2}$, and then electrochemically tested in 1.0 M KOH/0.5 M H_2SO_4 solution. The stability test was carried out by dropping the catalyst onto the carbon paper (Tory, TGP-H-060) and maintaining the current density at 10 $mA \cdot cm^{-2}$. The amount of hydrogen produced in the electrolytic cell was collected by the drainage method.

Calculation of the electrochemically surface area

The electrochemically active surface area (ECSA) of the as synthesized samples without carbon black was estimated by the cyclic voltammetry (CV) measurements1. The electrochemical double-layer capacitance was tested from 0.1 to 0.3 V (vs RHE) in 1M KOH. solution for the HER or OER process at different scan rates (20, 40, 60, 80, 100, 120 $mV \cdot s^{-1}$). The difference between the anode and cathode currents was plotted linearly against the scan rate, with the slope corresponding to the electrochemical double-layer capacitance (C_{dl})

The ECSA was then estimated using the following equation:

$$ECSA = C_{dl} \cdot S / C_s$$

where S represents the real surface area of the smooth metal electrode, which was generally equal to the geometric area of the glassy carbon electrode ($S = 0.07065\ cm^2$). The specific capacitance (C_s) for a flat surface was generally considered to be 60

$\mu F \cdot cm^{-2}$. In this work, we also test the H_{upd} method for ECSA, in which all catalysts were scanned by CV in N_2-saturated 1 M KOH solution with a scan rate of 50 $mV \cdot s^{-1}$

Measurement of turnover frequency (TOF).

TOF ($H_2 \cdot s^{-1}$) is calculated by the following formula. TOF = $I/(2nF)$, where I is the current (A) during linear sweep voltammetry (LSV), F is the Faraday constant (96485.3 C mol^{-1}), and n is the number of active sites (mol). Factor 2 is based on the two-electron process of hydrogen evolution reaction.

HER FE

The HER FE of Ru-WC_{1-x} was calculated based on the following equation: $FE = neF/Q$, where e is the number of electrons transferred for generating H_2, Q is the total charge, n is the amount of generated H_2 (in moles) and F is the Faradaic constant.

Electrochemical measurements in AEM electrolyzer

The AEM testing is based on a recent protocol. First, the as-received ion-exchange-resin membrane (SustainionR37-50) was immersed into 1.0 M KOH for 24 h before the construction of the AEM electrolyzer. 0.5 Ru-WC_{1-x}, commercial 20% Pt/C were used as the cathode catalysts. The catalyst ink for Ru-WC_{1-x} was prepared in the same way as described above. 1.5 mg of 0.5 Ru-WC_{1-x} was deposited onto a catalyst-coated membrane with surface area 1×1 cm^2. The AEM electrolyzer was evaluated at 60 °C, using 1.0 M KOH as the electrolyte with a flowing rate of 40 $mL \cdot min^{-1}$. The RuO_2 on titanium foam was prepared as the anode for the electrolyzer. Prior to AEM testing, 10 cycles of cyclic voltammetry (CV) were conducted from 1.0 V to 1.5 V of cell voltage at a scan rate of 50 $mV \cdot s^{-1}$. Then the AEM electrolyzer was conducted at 2

$mA \cdot cm^{-2}$ for 5 min to stabilize. Subsequently, the electrolyzer was tested at 2, 10, 20, 50, 100, 200 $mA \cdot cm^{-2}$, and increased in 200 $mA \cdot cm^{-2}$ steps until reaching 1 $A \cdot cm^{-2}$ via a chronopotentiometry method, and the potential was recorded.

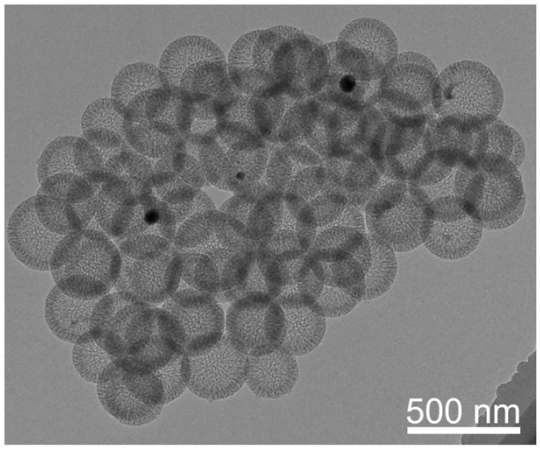

Fig. S1. TEM of CN.

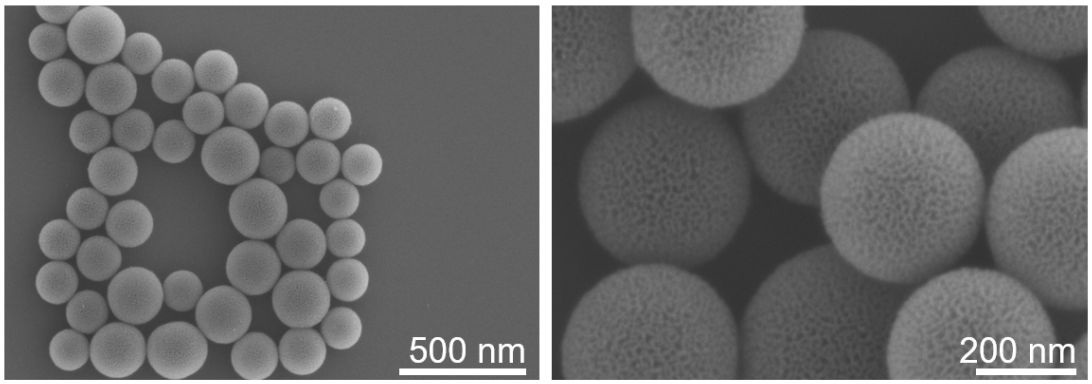

Fig. S2. SEM of CN.

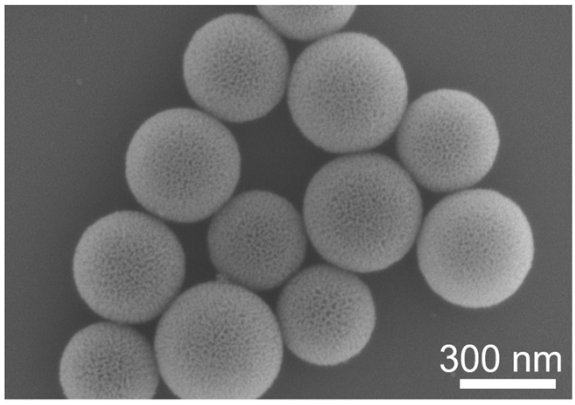

Fig. S3. SEM of Ru/CN.

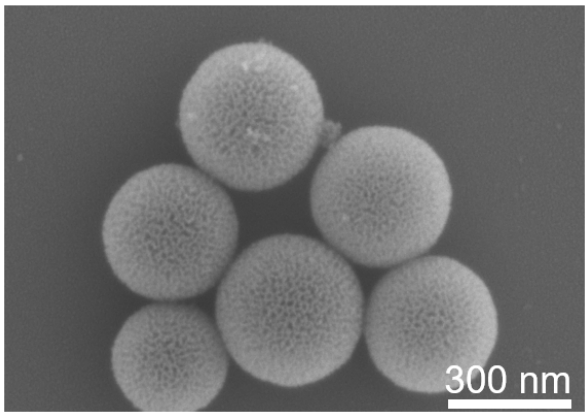

Fig. S4. SEM of Ru_3Ni/CN.

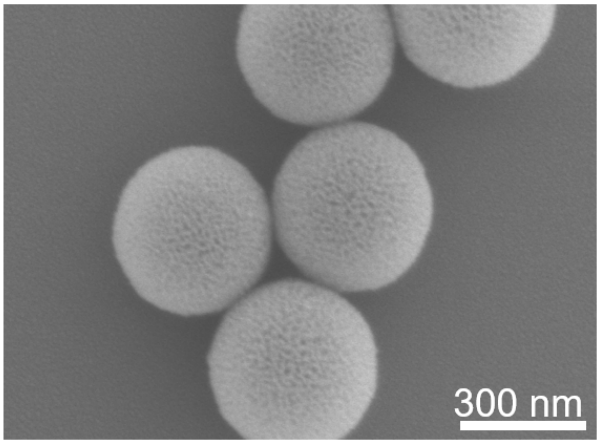

Fig. S5. SEM of Ni/CN.

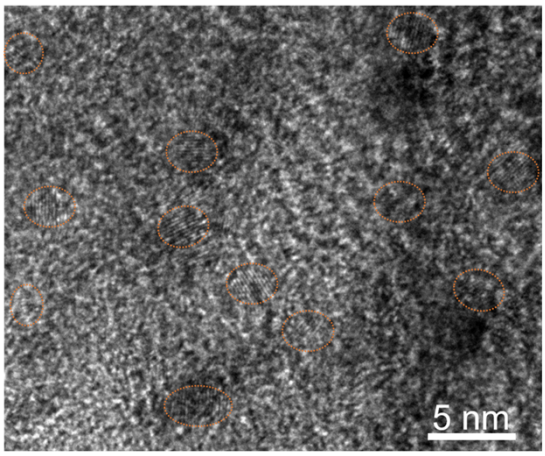

Fig. S6. Ru_3Ni nanoclusters on CN support.

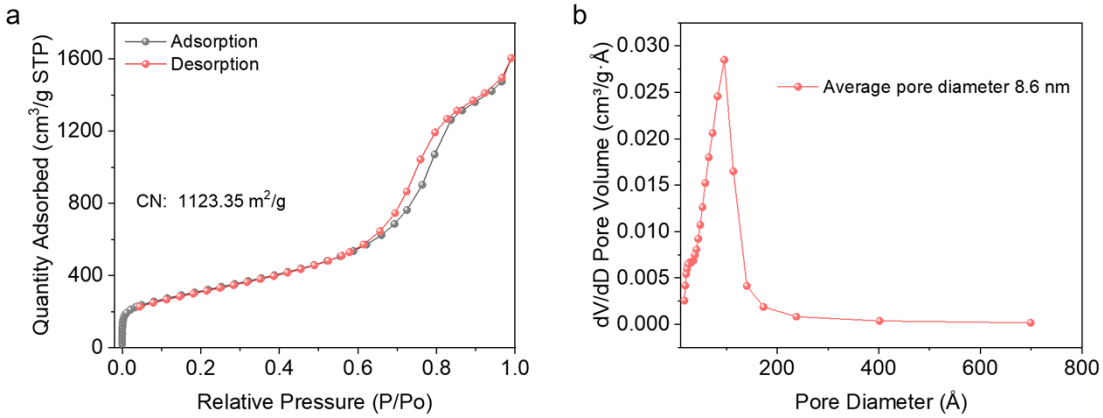

Fig. S7. (a) specific surface area of the CN. (b) The pore diameter distribution plots of the CN.

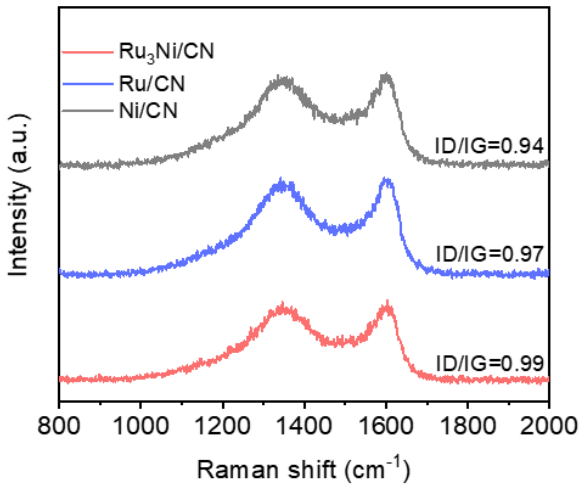

Fig. S8. Raman spectra of Ru3Ni/CN, Ru/CN and Ni/CN.

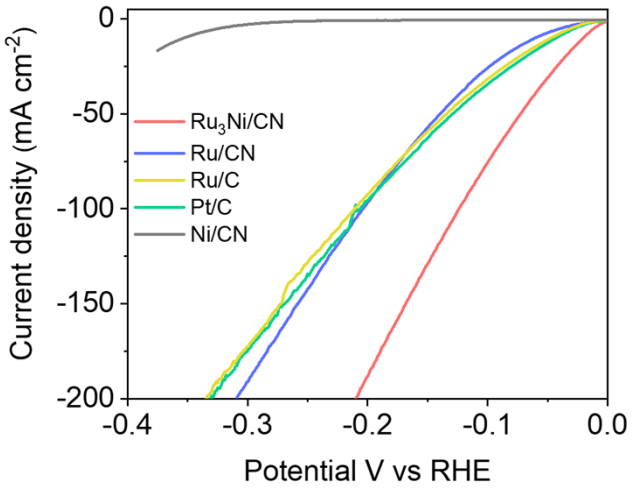

Fig. S9. The non-IR corrected LSVs for all electrocatalysts.

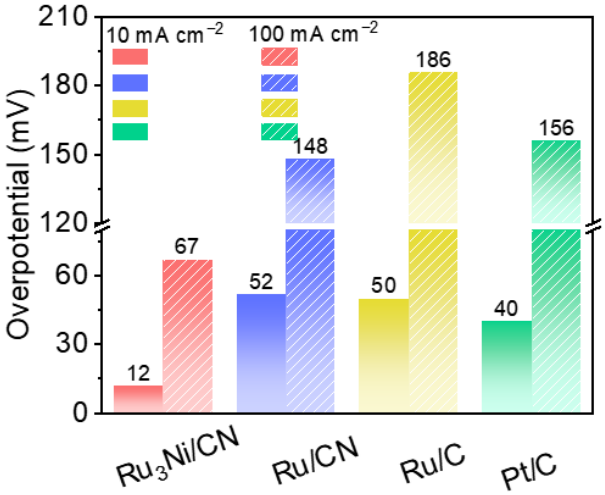

Fig. S10. Alkaline HER performances of RuNi. Corresponding overpotentials of Ru/CN, Ru/C, Ru3Ni/CN, and 20% Pt/C at the current densities of 10 mA cm^{-2} and 100 mA cm^{-2} in 1 M KOH.

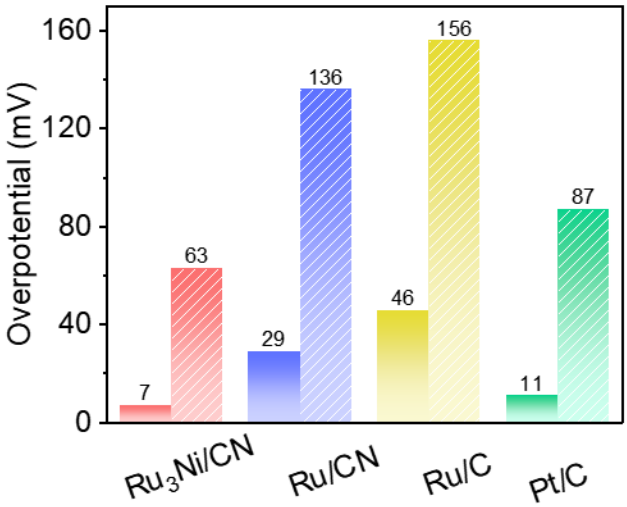

Fig. S11. Acidic HER performances of RuNi. Corresponding overpotentials of Ru/CN, Ru/C, Ru3Ni/CN, and 20% Pt/C at the current densities of 10 mA cm^{-2} and 100 mA cm^{-2} in 0.5 M H_2SO_4.

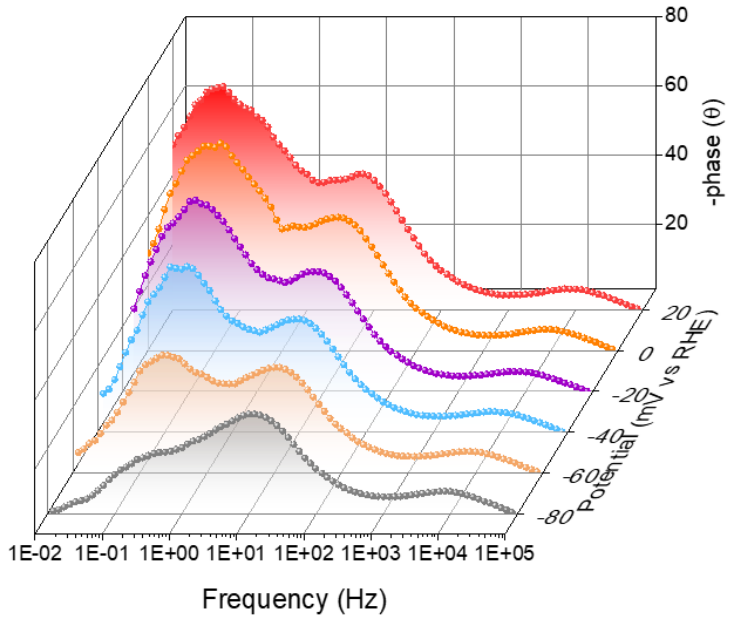

Fig. S12. Operando electrochemical impedance spectroscopy characterization. Bode plots of Ru/CN for HER in different potentials.

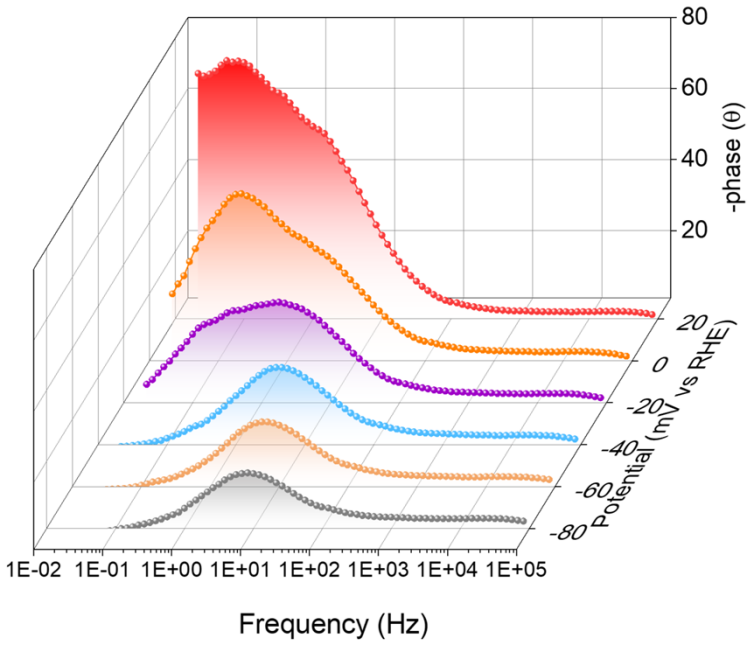

Fig. S13. Operando electrochemical impedance spectroscopy characterization. Bode plots of Ru_3Ni/CN for HER in different potentials.

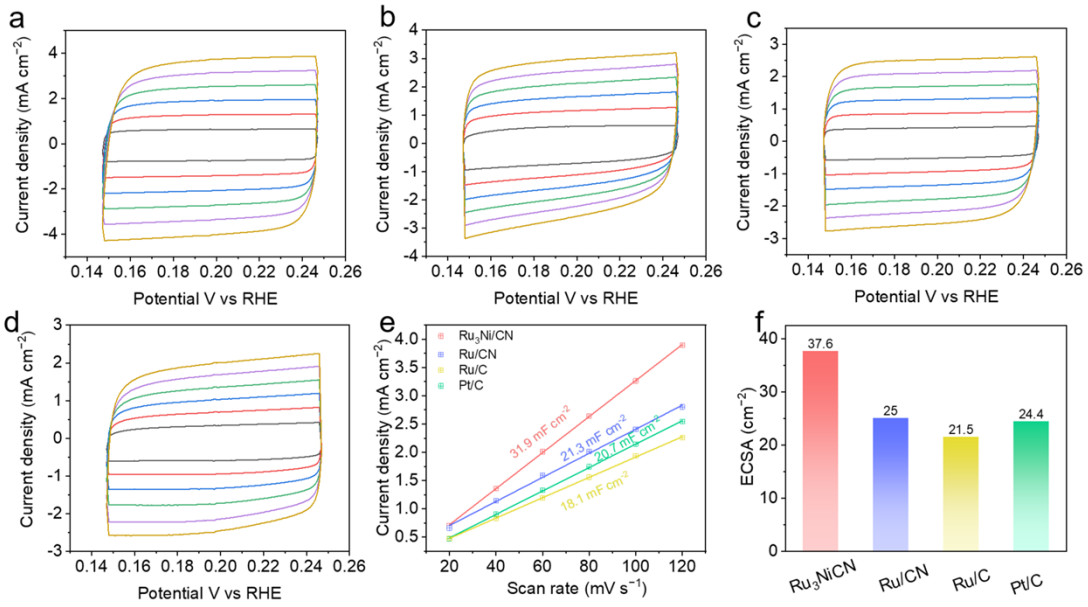

Fig. S14. ECSA measurements of electrocatalysts in 1M KOH. Electrochemical cyclic voltammetry scans recorded for (a) Ru_3Ni/CN, (b) Ru/CN, (c) Rui/C and (d) 20% Pt/C. Scan rates are 20, 40, 60, 80,100 and 120 mV·s^{-1}. (e) Linear fitting of the capacitive currents versus cyclic voltammetry scans for these catalysts. (f)The calculated ECSA values.

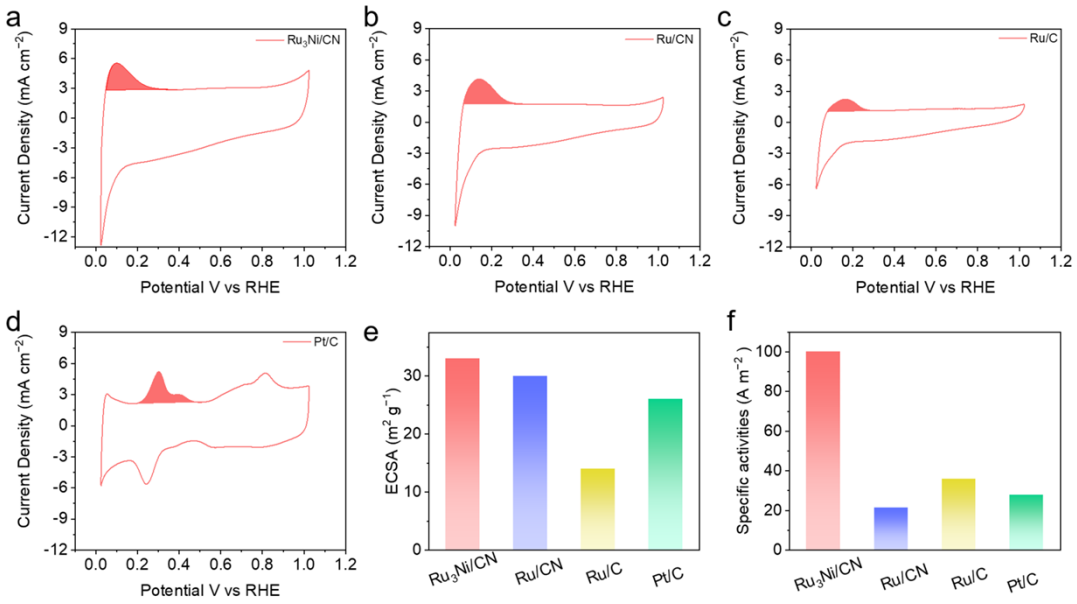

Fig. S15. ECSA measurements and specific activities based on Hupd method. The CV curves of (a) Ru_3Ni/CN, (b) Ru/CN, (c) Ru/C and (d) 20% Pt/C, the scan rate was controlled as 50 $mV \cdot s^{-1}$. (e) The corresponding ECSA values and (f) specific activities of Ru_3Ni/CN, Ru/CN, Ru/C and Pt/C derived from the H_{upd} method.

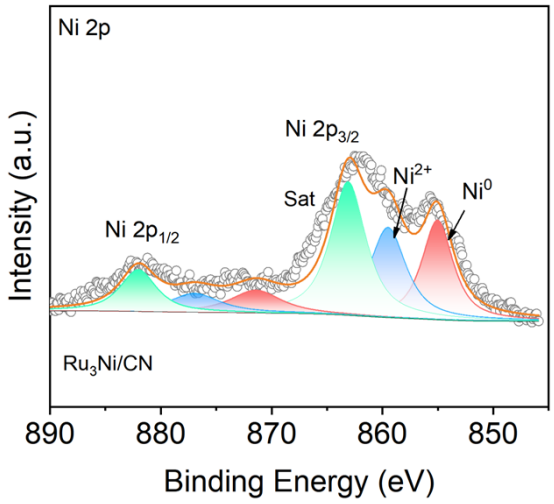

Fig. S16. XPS spectra of Ru_3Ni/CN after stability test. The Ni 2p XPS spectra after 100 h stability test at 10 mA cm^{-2}.

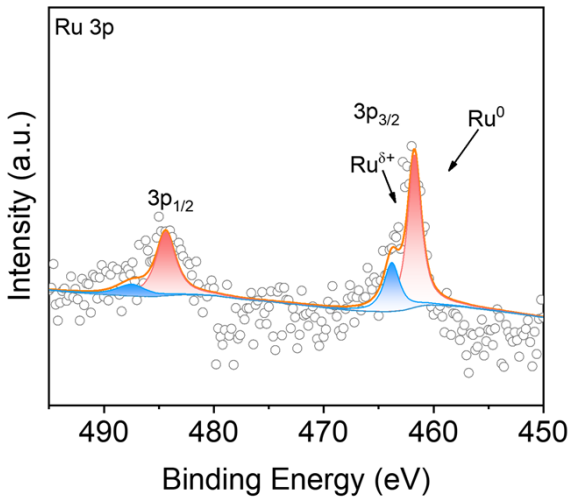

Fig. S17. XPS spectra of Ru_3Ni/CN after stability test. The Ru 3p XPS spectra after 100 h stability test at 10 mA cm^{-2}.

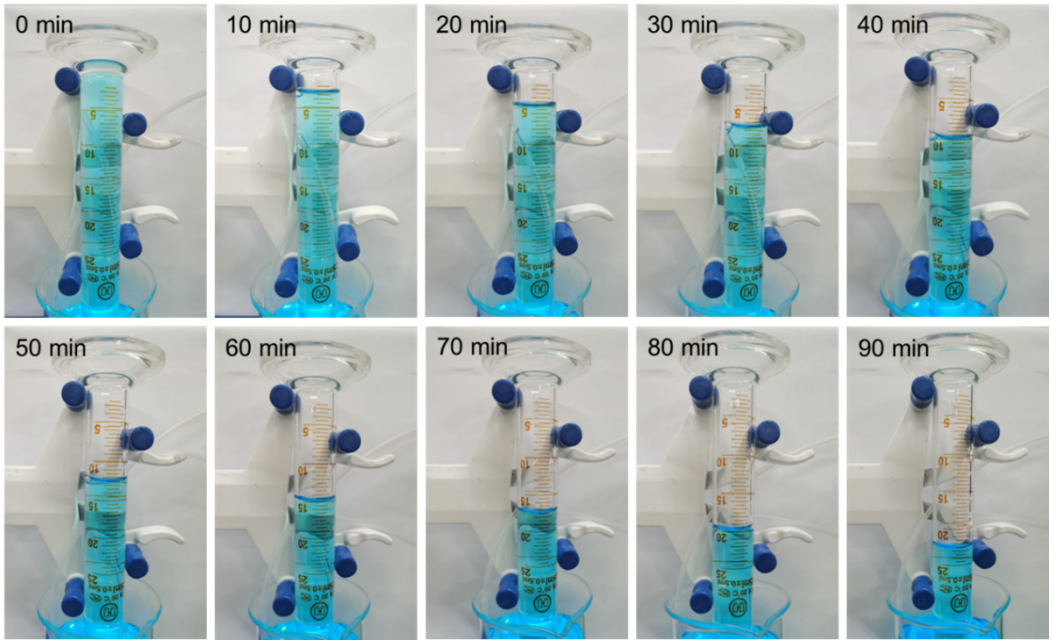

Fig. S18. H_2 collection volume in different time periods by drainage method.

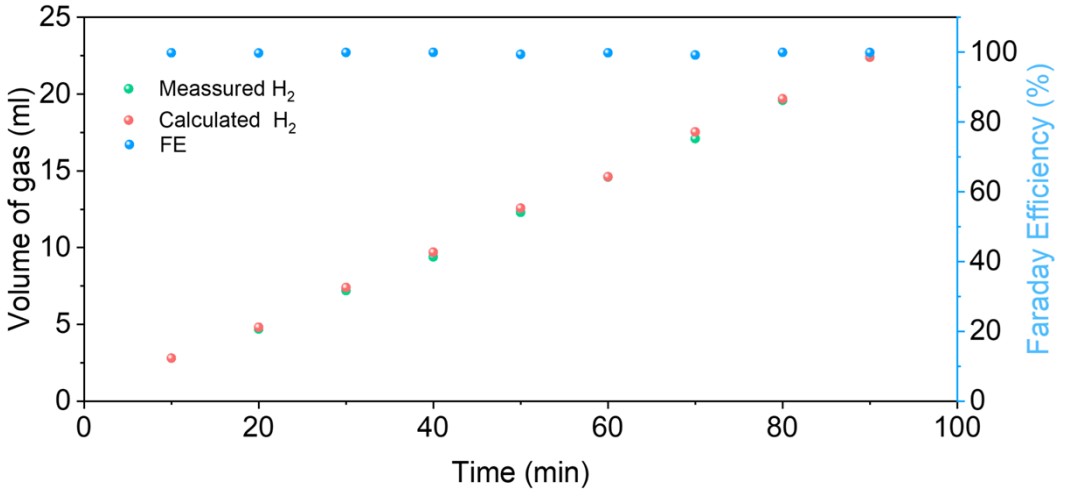

Fig. S19. The amount of H_2 about experimentally measured and theoretically calculated for Ru_3Ni/CN in 1.0 M KOH.

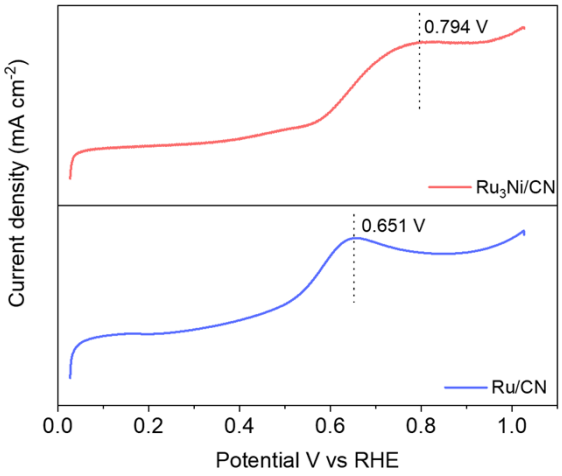

Fig. S20. LSV curves of Ru_3Ni/CN and Ru/CN in CO-saturated 1M KOH.

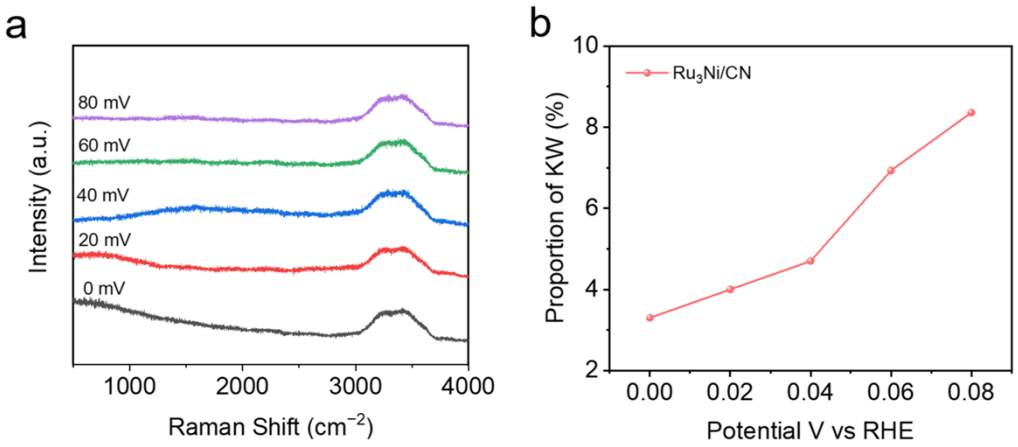

Fig. S21. (a)The operando Raman spectra of Ru_3Ni/CN under applied potentials in 1 M KOH solution, (b) Area ratio of dangling O-H bonds.

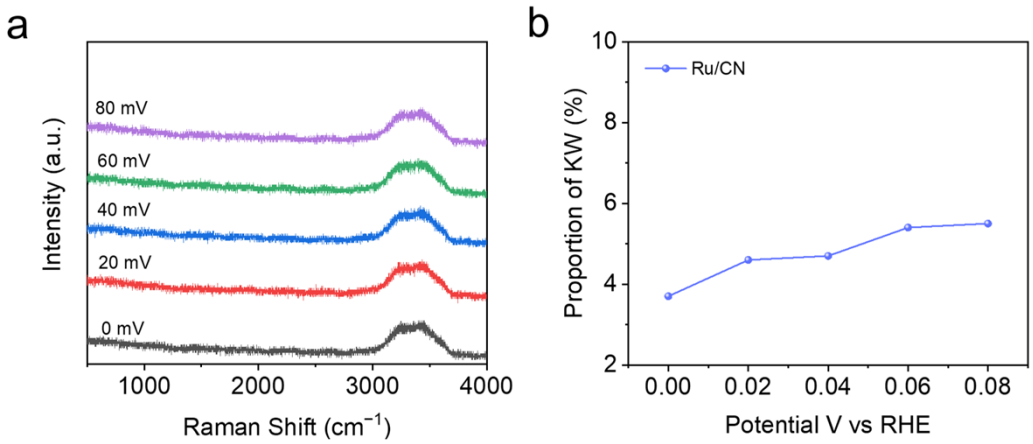

Fig. S22. (a)The operando Raman spectra of Ru/CN under applied potentials in 1 M KOH solution, (b) Area ratio of dangling O-H bonds.

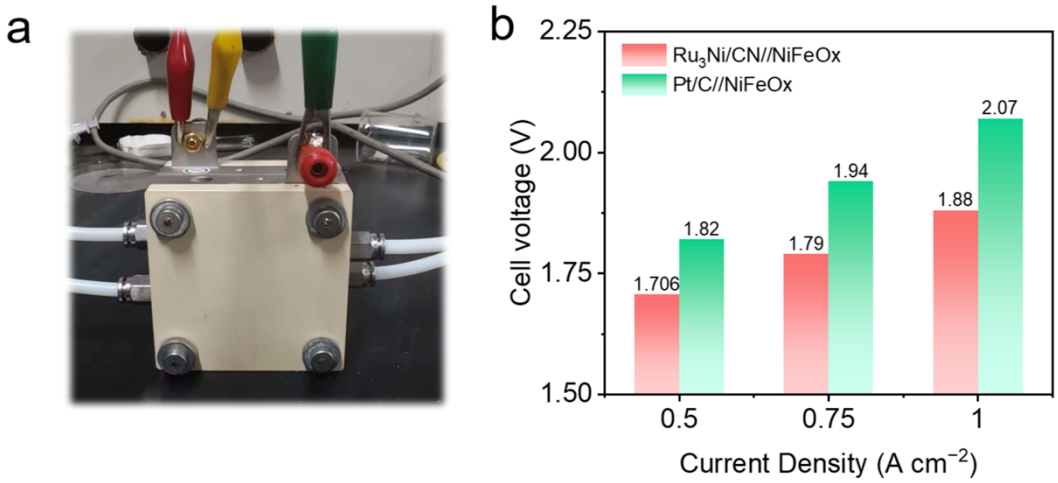

Fig. S23. (a) The AEMWE device, (b) Cell voltage of different current density.

Table S1 The contents of Ru and Ni measured by ICP

Sample	Ru(wt%)	Ni(wt%)	Ru:Ni molar ratio
Ni/CN	0	1.261	-
Ru/CN	7.153	0	-
Ru_3Ni/CN	7.432	1.326	3.01:1

Table S2. Summary of recently reported representative HER catalysts in alkaline electrolyte.

Catalyst	η_{10} (mV)	Tafel slope (mV dec^{-1})	Electrolyte	Ref
Ru_3Ni/CN	12	30.3	1 M KOH	This work
$CoRu\text{-}CoMoO_4$	49	27	1 M KOH	[1]
$Ru\text{-}NiCo_2S_4$	30	41	1 M KOH	[2]
$Ru/ZnRuO_2$	35	29.2	1 M KOH	[3]
a-Ru@GNL500	23	49	1 M KOH	[4]
Ru NRs/TiN	25	27.08	1 M KOH	[5]
$Ru@MoO(S)_3$	30	28	1 M KOH	[6]
$c/a\text{-}Ru/VO_x$	33	27	1 M KOH	[7]
CNT-V-Fe-Ru	38	41	1 M KOH	[8]
RuCoP	44	37	1 M KOH	[9]
$Ru@C_2N$	17	38	1 M KOH	[10]
RuNi/MoC	21	49.4	1 M KOH	[11]
Ru@CN-0.16	32	53	1 M KOH	[12]
$Ru\text{-}Ni_3N$	22.6	54	0.1 M KOH	[13]
$UP\text{-}RuNi_{SAs}/C$	9	37.6	1 M KOH	[14]
Ru/BCN	17	43	1 M KOH	[15]
$Mo–RuSe_2$	27	39	1 M KOH	[16]
RuGa/C-600	18	38.67	1 M KOH	[17]
$Ru@Co_3O_4$	9.8	18.6	1 M KOH	[18]
Ru/CNT	21	28.8	1 M KOH	[19]
Ru-FeCoP/FF	5	36.2	1 M KOH	[20]
Ru/G-S	15	52.3	1 M KOH	[21]
PtNi/Ru@CFN	25	29.87	1 M KOH	[22]
$MgO_x/MoO_y\text{-}Ru$	8.5	33.3	1 M KOH	[23]

Table S3. Summary of recently reported representative HER catalysts in acidic electrolyte.

Catalyst	η_{10} (mV)	Tafel slope (mV dec^{-1})	Electrolyte	Ref
Ru_3Ni/CN	7	30.6	0.5 M H_2SO_4	This work
I-PtZn@NPC	2.3	18.26	0.5 M H_2SO_4	[24]
PtRu/mCNTs	17	22.6	0.5 M H_2SO_4	[25]
Ru_2P@NPC	15	28	0.5 M H_2SO_4	[26]
Ru@MWCNT	13	27	0.5 M H_2SO_4	[27]
Ir@CON	13	30	0.5 M H_2SO_4	[28]
Ru_2P	13.4	27	0.5 M H_2SO_4	[29]
Ru/RuO_2-C	32	39.1	0.5 M H_2SO_4	[30]
RuP(L-RP)	19	37	0.5 M H_2SO_4	[31]
Pt_3Co@NCNT	42	27.2	0.5 M H_2SO_4	[32]
Pt-SA/Mo-L	31	31.1	0.5 M H_2SO_4	[33]
Pt/WCx	2	16	0.5 M H_2SO_4	[34]
Pt–Er/h-NC	25	17.1	0.5 M H_2SO_4	[35]
Pt/NBF-ReS_2/Mo_2CTx	29	24	0.5 M H_2SO_4	[36]
Pt1Ni_2Co@NC	26	30.14	0.5 M H_2SO_4	[37]
Ru/CNT	18	28.7	0.5 M H_2SO_4	[19]
PtNi/Ru@CFN	29	37.08	0.5 M H_2SO_4	[22]
Y−Ru/CNT/CC	27	44.3	0.5 M H_2SO_4	[38]
8Ru/FNPC	53.8	55.4	0.5 M H_2SO_4	[39]
RuRuO_2@Co/CNF	40	71.7	0.5 M H_2SO_4	[40]

Table S4. Comparison of the AEMWE performances of Ru_3Ni/CN with the reported Pt, Ru and non-noble based electrocatalysts.

Catalyst	E@0.5 A cm^{-2} (V)	Reference
Ru_3Ni/CN	1.706	This work
Pt1/CoHPO	1.722	[41]
Cl-Pt/LDH	1.787	[42]
Pt-AC/Cr-N-C	1.78	[43]
Pt-Ru SWNT	1.813	[44]
Ru/NDC-4	1.863	[45]
UP-$RuNi_{SAs}$/C	1.70	[14]
Pt@S-NiFe LDH	2.5	[46]
Ni_2Mo_3N	1.96	[47]
Ni_3S_2/Cr_2S_3	1.831	[48]
Pt–$MoAl_{1-x}B$	1.85	[49]
Pt1/$Co(OH)_2$	2.03	[50]
NA-Ru_3Ni/C	1.86	[51]
RuCo@$Ru_{SA}Co_{SA}$ NMC	1.93	[52]
PtNiNb	1.86	[53]

References

[1] H. Tong, S. Xu, X. Zheng, M. Qi, J. Zhu, D. Li, D. Jiang, Small, 2024, **21**,2409159.

[2] H. Su, S. Song, Y. Gao, N. Li, Y. Fu, L. Ge, W. Song, J. Liu, T. Ma, Advanced Functional Materials, 2021, **32**, 2109731.

[3] X. Zhang, Z. Su, D. Xiang, W. Xu, Q. Guo, Y. Fan, X. Kang, Y. Sheng, F. Zheng, W. Chen, Advanced Functional Materials, 2024, **34**, 202409306.

[4] G.M. Karim, A. Patra, S.K. Deb, H. Upadhya, S. Das, P. Mukherjee, W. Ahmad, N. Barman, R. Thapa, N.V. Dambhare, A.K. Rath, J. Das, U. Manna, R.R. Urkude, Y. Oh, U.N. Maiti, Advanced Functional Materials, 2024, **34**, 2315460.

[5] Y. Yang, D. Wu, R. Li, P. Rao, J. Li, P. Deng, J. Luo, W. Huang, Q. Chen, Z. Kang, Y. Shen, X. Tian, Applied Catalysis B: Environmental, 2022, **31**, 7121796.

[6] D. Chen, R. Yu, D. Wu, H. Zhao, P. Wang, J. Zhu, P. Ji, Z. Pu, L. Chen, J. Yu, S. Mu, Nano Energy, 2022, **100**, 107445.

[7] Z. Tao, H. Zhao, N. Lv, X. Luo, J. Yu, X. Tan, S. Mu, Advanced Functional Materials, (2024), **34**, 202312987.

[8] T. Gao, X. Tang, X. Li, S. Wu, S. Yu, P. Li, D. Xiao, Z. Jin, ACS Catalysis, 2022 **13**, 49-59.

[9] S. Liu, Z. Li, Y. Chang, M. Gyu Kim, H. Jang, J. Cho, L. Hou, X. Liu, Angewandte Chemie International Edition, 2024, **63** 202400069.

[10] J. Mahmood, F. Li, S.-M. Jung, M.S. Okyay, I. Ahmad, S.-J. Kim, N. Park, H.Y. Jeong, J.-B. Baek, Nature Nanotechnology, 2017, **12**, 441-446.

[11] X. Fan, B. Li, C. Zhu, F. Yan, Y. Chen, Nanoscale, 2023 **15**, 16403-16412.

[12] J. Wang, Z. Wei, S. Mao, H. Li, Y. Wang, Energy & Environmental Science, 2018, **11**, 800-806.

[13] Z. Liang, H. Liu, S. Huang, M. Xing, Z. Li, S. Wang, L. Yang, D. Cao, Journal of Materials Chemistry A, 2023, **11**, 849-857.

[14] R. Yao, K. Sun, K. Zhang, Y. Wu, Y. Du, Q. Zhao, G. Liu, C. Chen, Y. Sun, J. Li, Nature Communications, 2024, **15**, 2218.

[15] B Li, W Liu, M. Du, A. Li, X. Sun, J. Feng, J. Chen, D. Wan, H. Zhang, Journal of Materials Chemistry A, 2025 **13**, 27673–27680.

[16] Y. Ding, J. Zhu, M. Jiang, X. Zhan, J. Qin, X. Jiang, S. Wang, T. Meng, M. Cao, Journal of Materials Chemistry A, 2025, **13**, 8456–8465.

[17] C. Yang, L. An, Z. Mi, G. Wang, C. Zhang, W. Kong, J. Yang, L. Xiao, L. Zhuang, D, Wang, Journal of Materials Chemistry A, 2025, 13, 7158–7167.

[18] J. Wang, D. Wang, Z. He, M. Yan, Y. Xiang, H. Li, L. Xu, J. Li, Energy & Environmental Materials, 2025, **0**, e70172.

[19] X. Zhang, X. Lian, H. Jiao, Y. Wang, H. Li, X. Chang, Y. Li, J. Zhang, X. He, Advanced Functional Materials, 2025, **35**, 2508730.

[20] L. Zhan, Y. Liu, G. Zhou, K. Liu, Y. Du, L. Wang, Green Chemistry, 2025, **27**, 2417–2426.

[21] H. Wu, Z. Rao, Y. Luan, X. Jiang, L. Li, Y. Lian, Small, 2025, **21**, e10889.

[22] Y. Feng, Y. Wei, B. Wu, J. Li, Q. Dong, X. Li, Y. Wang, Q. Liu, Q. Ma, J. Zhang, W. Li, G. Chen, J. Huang, F. Zhang, Advanced Energy Materials, 2025, **15**, e03878.

[23] F. Tian, S. Geng, M. Li, L. Qiu, F. Wu, L. He, J. Sheng, X. Zhou, Z. Chen, M. Luo, Hu Liu, Y. Yu, W. Yang, S. Guo, Advanced Materials, 2025, **37**, 2501230.

[24] M. Wang, Z. Shi, W. Shi, J. Jiang, J. Lan, Li, Y. Yan, Z. Liu, L. Fu, X. Liu, S. Sang, Y. Hu, J. Zhou, Advanced Materials, 2025, **37**, 2501230.

[25] B. Pang, X. Liu, T. Liu, T. Chen, X. Shen, W. Zhang, S. Wang, T. Liu, D. Liu, T. Ding, Z. Liao, Y. Li, C. Liang, T. Yao, Energy & Environmental Science, 2022, **15**, 102-108.

[26] T. Liu, B. Feng, X. Wu, Y. Niu, W. Hu, C.M. Li, ACS Applied Energy Materials, 2018 **1**, 3143-3150.

[27] D.H. Kweon, M.S. Okyay, S.-J. Kim, J.-P. Jeon, H.-J. Noh, N. Park, J. Mahmood, J.-B. Baek, Nature Communications, 2020, **11**, 1278.

[28] J. Mahmood, M.A.R. Anjum, S.H. Shin, I. Ahmad, H.J. Noh, S.J. Kim, H.Y. Jeong, J.S. Lee, J.B. Baek, Advanced Materials, 2018, **30**, 201805606.

[29] X. Jin, H. Jang, N. Jarulertwathana, M.G. Kim, S.-J. Hwang, ACS Nano, 2022, **16**, 16452-16461.

[30] M. Wu, Y. Fan, Y. Huang, D. Wang, Y. Xie, A. Wu, C. Tian, Nano Research, (2024) **17**, 6931-6939.

[31] J. Yu, Y. Guo, S. She, S. Miao, M. Ni, W. Zhou, M. Liu, Z. Shao, Advanced Materials, 2018, **30**, 201800047.

[32] S. Liu, W. Cao, J. Wu, E. Hu, J. Zhang, X. Gao, Z. Chen, ACS Applied Materials & Interfaces, 2023, **16**, 520-529.

[33] H. Yuan, D. Jiang, Z. Li, X. Liu, Z. Tang, X. Zhang, L. Zhao, M. Huang, H. Liu, K. Song, W. Zhou, Advanced Materials, 2023, **36**, 202305375.

[34] T. Ma, H. Cao, S. Li, S. Cao, Z. Zhao, Z. Wu, R. Yan, C. Yang, Y. Wang, P.A. van Aken, L. Qiu, Y.G. Wang, C. Cheng, Advanced Materials, 2022, **34**, 202206368.

[35] G. Chen, W. Chen, R. Lu, C. Ma, Z. Zhang, Z. Huang, J. Weng, Z. Wang, Y. Han, W. Huang, Journal of the American Chemical Society, 2023, **145**, 22069-22078.

[36] M. Yi, N. Li, B. Lu, L. Li, Z. Zhu, J. Zhang, Energy Storage Materials, 2021 **42**, 418-429.

[37] N. Zhou, R. Zhang, R. Wang, Y. Li, Chemical Engineering Journal, 474 (2023).

[38] H. Cai, N. Jiang, L. Xiong, F. Shang, Y. Tang, X. Zhang, C. Liang, D. Su, S. Yang, ACS Applied Materials & Interfaces, 2025, **17**, 63448−63456.

[39] J. Guo, R. Ding, Y. Li, J. Xie, Q Fang, M. Yan, Y. Zhang, Z. Yan, Z. Chen, Y. He, X. Sun, E. Liu, Small, 2024, **20**, 202403151.

[40] N. Zheng, B. Yang, J. Xie, J. Hu, Z. Lu, Y. Cao, Chemical Engineering Journal, 2026, **529**, 173158.

[41] L. Zeng, Z. Zhao, F. Lv, Z. Xia, S.-Y. Lu, J. Li, K. Sun, K. Wang, Y. Sun, Q. Huang, Y. Chen, Q. Zhang, L. Gu, G. Lu, S. Guo, Nat. Commun. 2022, **13**, 3822.

[42] T. Zhang, J. Jin, J. Chen, Y. Fang, X. Han, J. Chen, Y. Li, Y. Wang, J. Liu, L. Wang, Nat. Commun. 2022, **13**, 6875.

[43] L. Zeng, Z. Zhao, Q. Huang, C. Zhou, W. Chen, K. Wang, M. Li, F. Lin, H. Luo, Y. Gu, L. Li, S. Zhang, F. Lv, G. Lu, M. Luo, S. Guo, J. Am. Chem. Soc. 2023, **145**, 21432-21441.

[44] F.S.M. Ali, R.L. Arevalo, M. Vandichel, F. Speck, E.-L. Rautama, H. Jiang, O. Sorsa, K. Mustonen, S. Cherevko, T. Kallio, Appl. Catal. B Environ. 2022, **315**, 121541.

[45] J.-T. Ren, L. Chen, H.-Y. Wang, W.-W. Tian, X. Zhang, T.-Y. Ma, Z. Zhou, Z.-

Y. Yuan, Appl. Catal. B Environ. 2023, **327**, 122466.

[46] H. Lei, Q. Wan, S. Tan, Z. Wang, W. Mai, Adv. Mater. 2023, **35**, 2208209.

[47] J.Y. Zhao, Z.X. Lou, L.Y. Xue, Y. Ding, X. Li, X. Wu, Y. Liu, H.Y. Yuan, H.F. Wang, P.F. Liu, S. Dai, H.G. Yang, J. Mater. Chem. A. 2023, **11**, 7256–7263.

[48] H.Q. Fu, M. Zhou, P.F. Liu, P. Liu, H. Yin, K.Z. Sun, H.G. Yang, M. Al-Mamun, P. Hu, H.-F. Wang, H. Zhao, J. Am. Chem. Soc. 2022, **144**, 6028-6039.

[49] S.J. Park, T.H. Nguyen, D.T. Tran, V.A. Dinh, J.H. Lee, N.H. Kim, Energy Environ. Sci., 2023, **16**, 4093-4104.

[50] D. Cao, Z. Zhang, Y. Cui, R. Zhang, L. Zhang, J. Zeng, D. Cheng, Angew. Chem. Int. Ed. 2023, **62**, e202214259.

[51] L. Gao, F. Bao, X. Tan, M. Li, Z. Shen, X. Chen, Z. Tang, W. Lai, Y. Lu, P. Huang, C. Ma, S.C. Smith, Z. Ye, Z. Hu, H. Huang, Energy Environ. Sci., 2023, **16**, 285–294.

[52] X. Wang, H. Yao, C. Zhang, C. Li, K. Tong, M. Gu, Z. Cao, M. Huang, H. Jiang, Adv. Funct. Mater. 2023, **33**, 2301804.

[53] J. Gu, L. Li, Y. Xie, B. Chen, F. Tian, Y. Wang, J. Zhong, J. Shen, J. Lu, Nat. Commun. 2023, **14**, 5389.